In Silico Screening of Two-Photon Absorption Properties of a Large Set of Bis-Difluoroborate Dyes

Iryna Knysh, Mohammed Bin Jassar, Borys Ośmialowski, Robert Zaleśny, Denis Jacquemin

▶ **To cite this version:**

Iryna Knysh, Mohammed Bin Jassar, Borys Ośmialowski, Robert Zaleśny, Denis Jacquemin. In Silico Screening of Two-Photon Absorption Properties of a Large Set of Bis-Difluoroborate Dyes. ChemPhotoChem, 2022, 6 (10), pp.e202200137. 10.1002/cptc.202200137 . hal-03868117

HAL Id: hal-03868117
https://ifp.hal.science/hal-03868117

Submitted on 6 Dec 2022

HAL is a multi-disciplinary open access archive for the deposit and dissemination of scientific research documents, whether they are published or not. The documents may come from teaching and research institutions in France or abroad, or from public or private research centers.

L'archive ouverte pluridisciplinaire **HAL**, est destinée au dépôt et à la diffusion de documents scientifiques de niveau recherche, publiés ou non, émanant des établissements d'enseignement et de recherche français ou étrangers, des laboratoires publics ou privés.

Distributed under a Creative Commons Attribution - NonCommercial 4.0 International License

Check for updates

23670932, 2022, 10, Downloaded from https://chemistry-europe.onlinelibrary.wiley.com/doi/10.1002/cptc.202200137 by Ifp Energies Nouvelles Compabilité Fournisseurs, Wiley Online Library on [09/11/2022]. See the Terms and Conditions (https://onlinelibrary.wiley.com/terms-and-conditions) on Wiley Online Library for rules of use; OA articles are governed by the applicable Creative Commons License

Special Collection

In Silico Screening of Two-Photon Absorption Properties of a Large Set of Bis-Difluoroborate Dyes

Iryna Knysh,*[a] Mohammed Bin Jassar,[b] Borys Ośmiałowski,[c] Robert Zaleśny,*[d] and Denis Jacquemin*[a]

Dedicated to Professor Szczepan Roszak on the occasion of his 70th birthday

In this work we strive to unravel the relationships between the two-photon absorption (2PA) cross-sections and structural modifications in an extended panel (280 compounds) of large difluoroborate dyes. More specifically, we use theoretical tools based on Time-Dependent Density Functional Theory (TD-DFT), to predict the one and two-photon absorption properties of all compounds. The BF_2-carrying dyes usually posses a great interest for 2PA bioapplications as smartly designed BF_2-derivatives show good photophysical properties and high quantum yields in aqueous medium. For practical applications, it is important to maximize their 2PA response as well as absorption wavelength. This is why we explore here various strategies for maximizing the 2PA cross-section: core modifications, multi-branching, variation of the nature and length of the π-conjugated linkers, addition of various donor and acceptor substituents. Our results suggest that large values of 2PA cross-section and redshifted absorption wavelength can be achieved for all studied cores by using the vinylene-type linkers and asymmetrical substitution with at least one strong peripheral donor group.

Introduction

2PA was theoretically predicted in 1931 by Göppert-Mayer (GM),[1] and subsequently, experimentally observed by Kaiser and Garrett thirty years later.[2] 2PA is a non-linear process, with quadratic dependence on the light intensity, in which two photons, fulfilling the resonance condition, are simultaneously absorbed to reach an excited state. This fascinating phenomenon paves the way to a broad variety of applications, including 3D microfabrication,[3,4] optical data-storage,[5] optical power limiting,[6] 2PA microscopy,[7] bioimaging,[8] and photodynamic therapy.[9] Organic molecules occupy the leading spot in the 2PA field, especially for bioimaging and 2PA microscopy, due to several beneficial properties: biocompatibility, low toxicity, and the ease of functionalization allowing achieving tunable properties. Thanks to long-standing developments of computational chemistry methods, these methods now stand as very useful tools to evaluate 2PA properties and perform screening of large set of molecules in order to find the best candidates for 2PA applications.[10–23] For instance, owning to the work of Hättig and co-workers[12,13] 2PA cross sections (σ^{2PA}, measured in GM units), the key figures of merit, can be predicted by Coupled Cluster (CC) response theory. This has been implemented in the Dalton program package[24,25] for a variety of CC methods (up to the accurate third-order variant, CC3). Likewise, Nanda and Krylov[18] developed the theory for calculating 2PA cross section within the Equation-of-Motion formulation of CCSD, and implemented this approach in the Q-Chem program.[26] Although the latter algorithm uses both the resolution-of-the-identity (RI) and Cholesky decomposition (CD) for the electron-repulsion integrals in order to reduce the computational resources needed, practical applications remain limited to molecules containing *ca.* 30 atoms with a diffuse double-ζ basis set.[18,27] The Turbomole program[28] also allows computing σ^{2PA} using the second-order CC scheme (CC2), in an approach proposed by Friese *et al.*[16] As a result of the implementation of the RI approximation, RI-CC2 simulations are available for compounds with up to *ca.* 70 atoms with a double-ζ basis set[16] and such approach is often used to benchmark TD-DFT, though the actual accuracy of CC2 for 2PA remains somewhat unsettled. Nevertheless, the most popular and computationally efficient method for computing 2PA properties remains TD-DFT with implementation in several codes including GAMESS US, Dalton, and Turbomole.[14,17,20,24,25,29] In the TD-DFT framework, it is no surprise that the relative performances of different exchange-

[a] I. Knysh, Prof. D. Jacquemin
Nantes Université, CNRS, CEISAM UMR 6230, F-44000 Nantes, France
E-mail: Iryna.Knysh@univ-nantes.fr
Denis.Jacquemin@univ-nantes.fr
[b] M. B. Jassar
IFP Energies Nouvelles, Thermodynamics and Molecular Modeling Department, 1 et 4 avenue de Bois-Préau, 92852 Rueil-Malmaison Cedex, France
[c] Dr. B. Ośmiałowski
Faculty of Chemistry, Nicolaus Copernicus University, Gagarina 7, PL-87100 Toruń, Poland
[d] Dr. R. Zaleśny
Faculty of Chemistry, Wrocław University of Science and Technology, Wyb. Wyspiańskiego 27, PL–50370 Wrocław, Poland
E-mail: Robert.Zalesny@pwr.edu.pl

Supporting information for this article is available on the WWW under https://doi.org/10.1002/cptc.202200137

Special Collection An invited contribution to a Special Collection celebrating the 5 Year Anniversary of ChemPhotoChem

© 2022 The Authors. ChemPhotoChem published by Wiley-VCH GmbH. This is an open access article under the terms of the Creative Commons Attribution Non-Commercial License, which permits use, distribution and reproduction in any medium, provided the original work is properly cited and is not used for commercial purposes.

© 2022 The Authors. ChemPhotoChem published by Wiley-VCH GmbH

23670932, 2022, 10, Downloaded from https://chemistry-europe.onlinelibrary.wiley.com/doi/10.1002/cptc.202200137 by Ifp Energies Nouvelles Compabilité Fournisseurs, Wiley Online Library on [09/11/2022]. See the Terms and Conditions (https://onlinelibrary.wiley.com/terms-and-conditions) on Wiley Online Library for rules of use; OA articles are governed by the applicable Creative Commons License

correlation functionals were assessed in several studies.[19,21–23] Even if range-separated functionals usually provide larger absolute errors in σ^{2PA} than semilocal and global hybrid functionals, these range-separated functional often accurately reproduce the relative trends (in a series of compounds) given by higher levels of theory (CC) or experimental approaches. Consequently, the range-separated CAM–B3LYP[30] functional is usually a reasonable choice for computing 2PA properties of large dyes. We note that vertical transition energies of boron-dipyrromethene (BODIPY) derivatives predicted by TD-DFT tend to overestimate the experimental absorption maxima.[31–33] Nevertheless, CAM–B3LYP is again able to provide reliable trends.[34] Moreover, the development of a generalized few-state model (GFSM) for 2PA by Alam *et al.*[35] and its further extension[36] provides tools for a better understanding of 2PA process *via* the decomposition of the two-photon transition strengths (δ^{2PA}, which is proportional to σ^{2PA}) into electronic structure parameters.

The above-described quantum-chemistry methods developments allow performing reliable *in silico* screening of organic 2PA dyes for several applications. The potential of 2PA probe candidates is usually characterized by their two-photon action cross-section, which is the product of σ^{2PA} and the fluorescence quantum yield (ϕ^{fl}).[37] In order to increase the efficiency of 2PA dyes both parameters, σ^{2PA} and ϕ^{fl}, should be maximized. This is challenging, *e.g.*, small rigid organic molecules might present large ϕ^{fl} but often suffer from insignificant σ^{2PA} values.[38] Several recent reviews highlighted different approaches to design efficient 2PA dyes based on a panel of structure-properties relations.[6,39,40] The common strategy is to use strong donor (D) and acceptor (A) moieties separated by a π-conjugated linker. This design approach leads to electronic transitions having an intramolecular charge transfer (ICT) character and such dyes typically possess high σ^{2PA} as well as redshifted absorption and emission bands.[6] It is worth to mention that 2PA dyes can be also characterized by the normalized 2PA cross-section, which is a ratio between σ^{2PA} and number of π-electrons (N_e). It is indeed preferable to have compact molecules possessing high values of σ^{2PA}. Another approach to optimize σ^{2PA} is to synthesize multi-branched molecules, a strategy that has been found successful with various cores.[40] By combining D and A groups with different cores and π-conjugated linkers one can obtain molecules with different symmetries: dipolar (D-π-A), quadrupolar (D-π-A-π-D, A-π-D-π-A), or octupolar, having three branches with D (A) substituents surrounding an A (D) core. For instance, the joint experiment-theory study of Albota *et al.* demonstrates that large σ^{2PA} can be achieved for quadrupolar structures due to symmetric charge redistribution upon excitation.[41] In another work, the enhancement of σ^{2PA} was achieved by adding the electron-withdrawing branches to a donor core, so as to deliver an octupolar-like structure. Moreover, by carrying out TD-DFT calculations and using the Frenkel exciton model (to connect the photophysical properties of the multi-branched chromophores to their single-branch counterparts) it was shown that the coherent coupling between the branches stands as a possible mechanism behind this increase.[42] We underline that such design strategy allows not only obtaining high 2PA cross-sections, but also maintaining large fluorescence quantum yield.

The famous BODIPY family encompasses very bright fluorescent dyes, that are notably popular in bio- and medicinal applications.[43] Adequately functionalized BODIPY molecules can be soluble in lipids,[44] and maintain good photophysical properties in water,[45,46] including high quantum yields.[47] The BF_2-group is a characteristic structural feature of these dyes - it keeps the molecular skeleton rigid and acts as an electron accepting unit. Other BF_2-carrying dyes might, of course, differ from the BODIPYs in terms of structure, but they still often exhibit excellent photophysical properties in both solution and in the solid state.[48–50] Additionally, the presence of BF_2-group also increases significantly 2PA cross-section as demonstrated by comparisons between BF_2-dyes and its precursor.[51] Moreover, the 2PA properties of BF_2-containing dyes can be tuned by various synthetic strategies.[52,53] For the purpose of the present study we designed three different series of dyes (**A**, **B**, and **C** see Figure 1) containing the difluoroborate electron-withdrawing moiety. Previously, some of us showed that structure similar to series **A** might yield quite large σ^{2PA}.[54] Thus, in this work we continue to explore the modifications of this core using theoretical tools and consider an extremely large palette of compounds. We investigate here the influence of breaking the conjugation between two BF_2-containing heterocycles in the acceptor core (series **B**). Moreover, we study the impact of adding an extra branch with various electron-withdrawing or electron-donating substituents to series **A** leading to unsymmetrical dyes (series **C**), contrasting with series **A** and **B**.

As a foreword of this theoretical work, let us briefly comment on the synthetic accessibility. The stepwise synthesis of series **A** should be rather straightforward. Indeed, the bis-amide, which is the mid-product in the synthesis of BF_2-dyes, was obtained during studies of other members of the borate family.[53,55] In contrast, obtaining series **B** would need more investigations. The selective reduction of the C=C bond within the pyrimidine core may be a challenging task, as other double bonds are present within the linkers. The first part of the synthesis of series **C** could be similar to that of series **A**. As long as the methyl group is present in position 4 of heterocycle its condensation with aldehydes should led to series **C**. Thus, for reaching **C**-derivatives, the presence of a CH_3 group in position 4, close to the nitrogen atom, of the heterocyclic ring is mandatory. We note that this position is synthetically preferable to the corresponding position 5 close to the left hand-side arm carrying R substituent. The studied compounds are derivatives of amides and their use in BF_2-complexation is well-described,[52,55,56] while the elongation of the linkers may be achieved through Wittig reaction that was already applied in similar cases.[55] We of course do not state here that all 280 compounds treated here would be straightforward to synthesize, just that the dye design is fulfilling some realism.

© 2022 The Authors. ChemPhotoChem published by Wiley-VCH GmbH

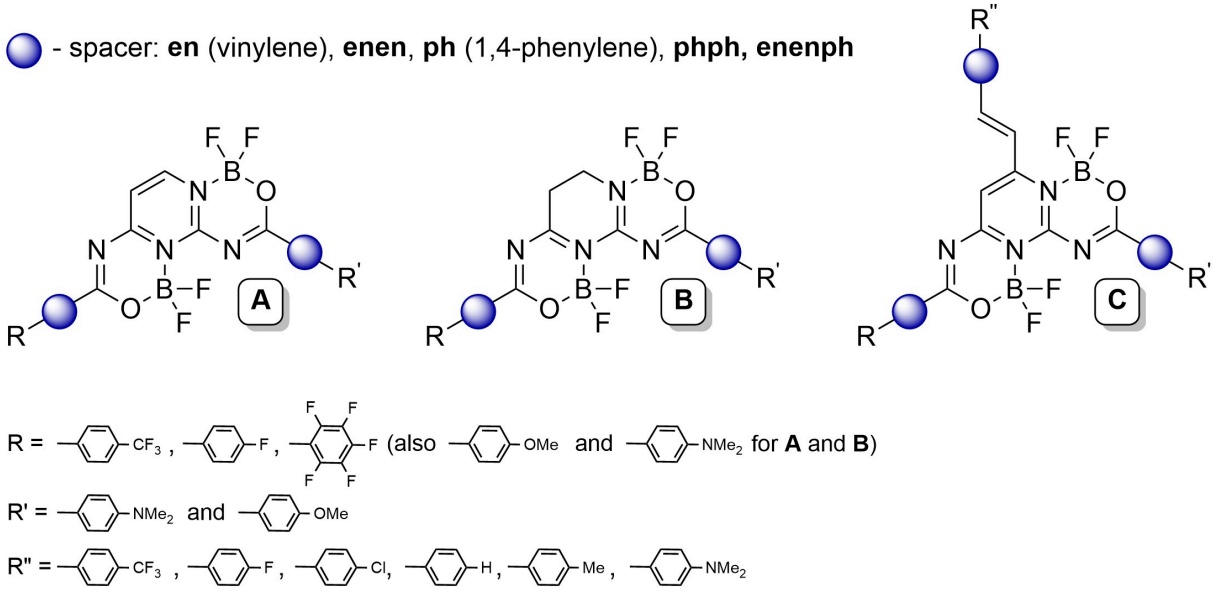

Figure 1. Structures of compounds studied in this work

Results and Discussion

Given the large number of systems treated here (280 dyes), all raw data are provided as a spreadsheet in the SI, and we focus on trends in the discussion below. Indeed, a molecule-per-molecule comparison would obviously not offer high clarity of presentation. In this work we study the photophysical properties corresponding to the S_0-S_1 transition, which is of $\pi\pi^*$ nature. Let us start with a comparison of one-photon absorption (1PA) and 2PA data obtained in the **A** and **B** series. Correlations between σ^{2PA} and one-photon absorption wavelength split by linker type for series **A** and **B** are presented in Figure 2. The corresponding graphs for the correlation between σ^{2PA}, the oscillator strength (*f*) and the CT parameters (D_{CT}, q_{CT} and μ_{CT}) can be found in Figure S1 in the SI. As can be seen in Figure 2 removing the conjugation between two BF_2-containing heterocycles (series **B**) slightly redshifts the 1PA wavelength and increases the 2PA cross-section as compared to the fully conjugated structure (series **A**). Additionally, we can see in Figure S1 an increase of all three CT parameters in derivatives of the **B** family as compared to their **A** counterparts. As a logical consequence, the oscillator strength undergoes the opposite evolution, as it tends to decrease in going from **A** to **B** (see Figure S1), but one clearly remarks a globally poor correlation between the magnitudes of *f* and σ^{2PA}, whereas for a given linker, larger σ^{2PA} values are correlated to stronger CT characters. Likewise, in Figure 2, one sees a general positive correlation between λ^{1PA} and σ^{2PA} for all linkers. One also notices that both **ph** (phenyl) and **phph** (bi-phenyl) groups typically yield rather small absorption wavelength, whereas the use of vinylene-containing linkers (**en**, **enen**, and **enenph**) redshifts the λ^{1PA}, which is the expected trend as double bonds yield more strongly conjugated structures than aromatic linkers. As anticipated as well, longer linkers induce bathochromic shifts in the vinylene series. However, this is not systematically the case when comparing **ph** and **phph** or **enen** to **enenph**. Furthermore, the big variation of **B**-derivatives in terms of CT parameters compared to their **A** counterparts is especially noticeable for **ph** and **phph** linkers, which results usually in the moderate increase of σ^{2PA}. In contrast, quite big changes in σ^{2PA}, D_{CT}, q_{CT}, and μ_{CT} can be seen passing from **A** to **B** for **en** and **enen**. One very interesting conclusion of Figure 2 is that some less conjugated linkers (like **phph**) might still deliver very large σ^{2PA}. This is consistent with the above observation that the **B** series 2PA responses exceed their **A** conterparts in several cases: maximizing the delocalization is not systematically beneficial for increasing σ^{2PA}. Finally, we note that Figure 2 can be roughly divided in two parts: the low response molecules ($\sigma^{2PA} < 200$ GM) and the high response ones ($\sigma^{2PA} > 200$ GM) with all linkers but **en** (except for a few molecules in the **B** series), giving access to both categories. We underline that the 200 GM threshold value corresponds to the median for molecules of **A** and **B** families considered together. Summarizing the above discussion, one can obtain large σ^{2PA} and redshifted λ^{1PA} in both series (**A** and **B**) using **enen** and **enenph** linkers while using **ph** and **phph** linkers results in increase of 2PA cross-section only.

While we can notice a moderate difference of 2PA cross-sections between **enen** and **enenph** linkers for series **A**, they deliver similar responses for series **B** (Figure 2). Hence, it is interesting to take a look at the normalized 2PA cross-section, σ^{2PA}/N_e. In Figure S1e the correlation between σ^{2PA} and σ^{2PA}/N_e is presented. Notably, in most cases **B**-derivatives have larger values of normalized cross-section as compared to their **A** counterparts. Importantly, Figure S1e shows that decreasing the conjugation in the core (**B** series) results in very large increase of 2PA cross-sections using the smallest linkers in the

© 2022 The Authors. ChemPhotoChem published by Wiley-VCH GmbH

23670932, 2022, 10, Downloaded from https://chemistry-europe.onlinelibrary.wiley.com/doi/10.1002/cptc.202200137 by Ifp Energies Nouvelles Compabilité Fournisseurs, Wiley Online Library on [09/11/2022]. See the Terms and Conditions (https://onlinelibrary.wiley.com/terms-and-conditions) on Wiley Online Library for rules of use; OA articles are governed by the applicable Creative Commons License

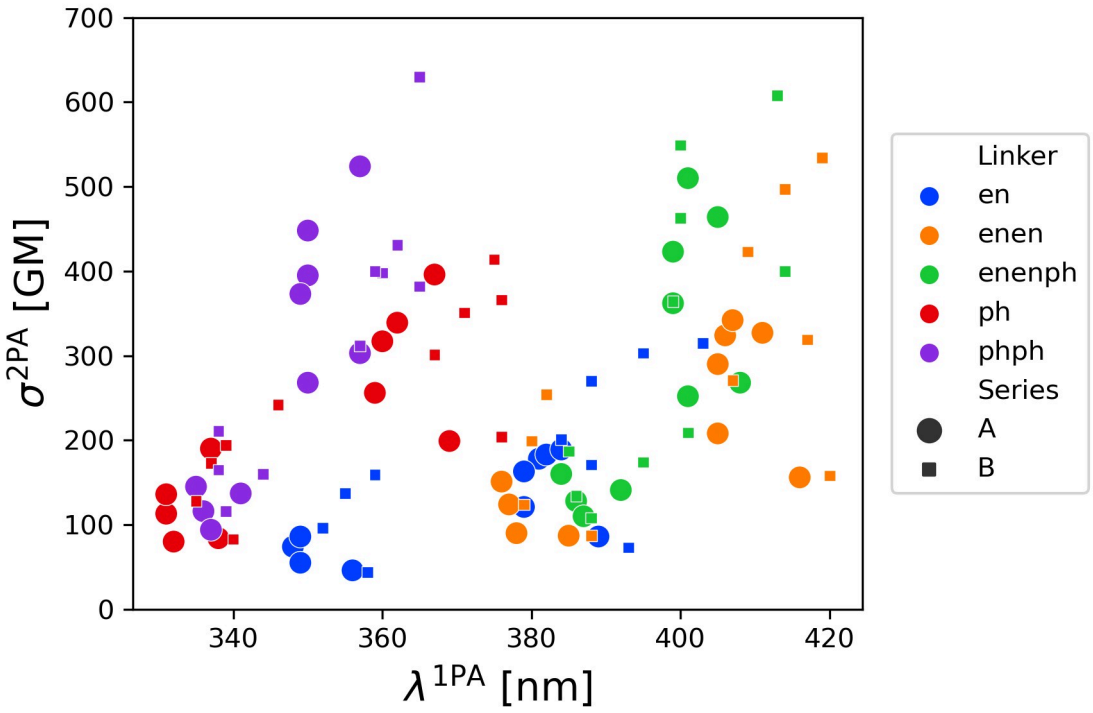

Figure 2. Correlation between λ^{1PA} and σ^{2PA} taking into account different linkers for series **A** and **B**, and considering all terminal groups.

series (**en** and **enen**), an outcome which correlates with the stronger CT character of these derivatives (see Figure S1).

The graphs in Figure 3 that focus on the impact of lateral substituents shed light on some of the above mentioned differences: the derivatives of Figure 2 with lower σ^{2PA} values mainly have a C_6H_4-OMe substituent (R′) while larger responses are obtained with the more potent amino group (C_6H_4-NMe_2). Obviously, the increase of 2PA cross-sections are related to the stronger donating ability of the dimethylamino group as compared to the methoxy moiety, given that the fluoroborate core acts as an acceptor. Moreover, the strategy with symmetrical donor substitution at the extremities, that is, the quadrupolar-like approach (D-π-A-π-D in series **A** and series **B**) seems to be less efficient than the antisymmetrical substitution with donor and acceptor groups placed in a dipolar-like arrangement. Indeed, it is seen in Figure 3 that the largest σ^{2PA}

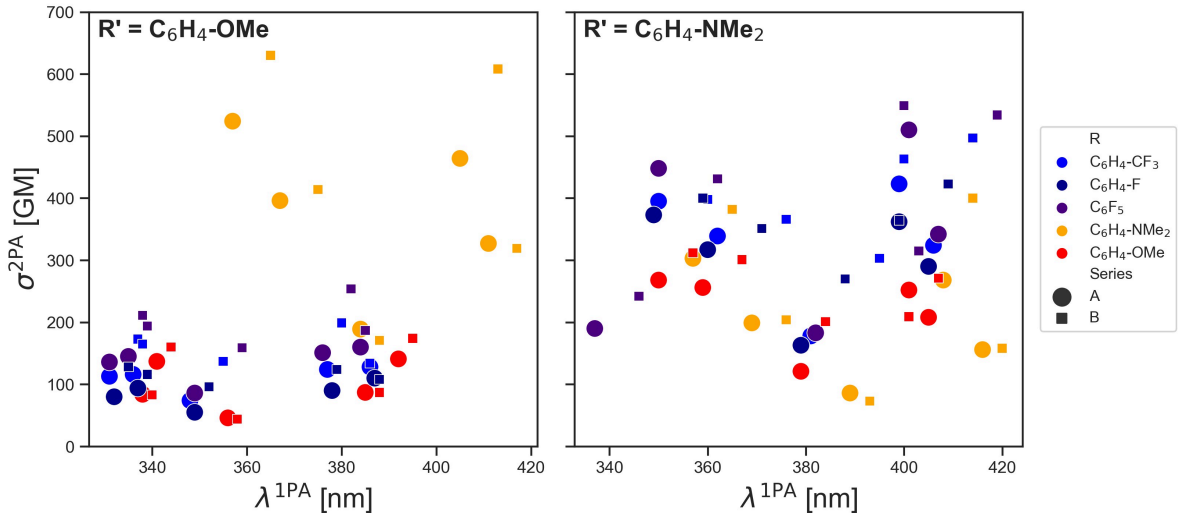

Figure 3. Relationship between λ^{1PA} and σ^{2PA} decomposed by R and R substituents in series **A** and **B**.

© 2022 The Authors. ChemPhotoChem published by Wiley-VCH GmbH

23670932, 2022, 10, Downloaded from https://chemistry-europe.onlinelibrary.wiley.com/doi/10.1002/cptc.202200137 by Ifp Energies Nouvelles Compabilité Fournisseurs, Wiley Online Library on [09/11/2022]. See the Terms and Conditions (https://onlinelibrary.wiley.com/terms-and-conditions) on Wiley Online Library for rules of use; OA articles are governed by the applicable Creative Commons License

are mostly achieved with R being a strong accepting group (C_6F_5) and R′ a strong donating group (C_6H_4-NMe_2). Nevertheless, in a few cases in both series, quite large 2PA cross-sections are also obtained with a pair of donor substituents (R = C_6H_4-NMe_2 and R′ = C_6H_4-OMe). To go further, we generated density difference plots for representative example in both series with different donor substitutions and the **enenph** linker (Table S1 and S2 in the SI). Clearly, one can see that additionally to decreasing the conjugation in the BF_2-core an increase of σ^{2PA} can be also promoted by a well designed asymmetric substitution. However, the increase is achieved with R = C_6H_4-NMe_2 and R′ = C_6H_4-OMe only, the reverse pattern is much less effective. This leads to the conclusion, that maximizing the σ^{2PA} in series **A** and **B** requires asymmetric substitution with at least one strong donor group.

Let us now compare the **A** and **C** series. These two structures differ by the presence of an additional π-conjugated branch bearing the extra R" substituent in the latter series. In order to preserve consistency between the **A** and **C** series we consider only accepting substituents for R (R = C_6H_4-CF_3, C_6H_4-F, C_6F_5) in series **A**. Correlation graphs between σ^{2PA} and λ^{1PA} for both series are presented in Figure 4. Figures showing the relationships between σ^{2PA}, *f*, CT parameters and normalized 2PA cross-section can be found in the SI (Figure S2). Clearly, we can observe in Figure 4 quite large redshifts of λ^{1PA} for series **C** as compared to series **A**, which is expected since an additional π-conjugated branch is present in the former derivatives increasing the delocalization. Similarly to the series **A** and **B**, the highest values of λ^{1PA} in series **C** are achieved with vinylene linkers (**en**, **enen**, and **enenph**) rather than aromatic ones (**ph** and **phph**). Although quite large σ^{2PA} can be obtained for both series and with both types of linkers, the **enen** and **enenph** bridges are superior to the **ph** and **phph** linkers in terms of 2PA cross-sections. Figure S2 additionally indicates that dyes of series **C** show larger D_{CT}, q_{CT} and μ_{CT} than **A**-derivatives when vinylene π-conjugated linkers are used, whereas the opposite is found for some molecules bearing **ph** and **phph** linkers. Similarly to series **A** and **B**, the same conclusion of better efficiency of vinylene linkers in terms of increasing both σ^{2PA} and λ^{1PA} therefore holds for series **C**.

It is particularly interesting to analyze the normalized 2PA cross-sections in the case of **C**-derivatives to quantify if the increase of the σ^{2PA} simply correlates with larger number of π-electrons in the system. The relationship between σ^{2PA} and σ^{2PA}/N_e can be found in Figure S2 in the SI. Generally, series **C** tends to have lower or almost the same values of σ^{2PA}/N_e as series **A**. Nevertheless, the highest values of both parameters are achieved for series **C** with the **enen** linker, the maximal σ^{2PA}/N_e response, ca. 20 GM, being however only slightly higher than the best value that can be reached with **B** compounds, ca. 19 GM. Thus, in case of series **C** the increase of σ^{2PA} is globally proportional to the molecule size.

Additionally, paralleling the above discussion it is also possible to split the compounds in Figure 4 into lower and higher response parts by using a σ^{2PA} = 300 GM threshold. However, in contrast to the series **A** and **B**, the difference in

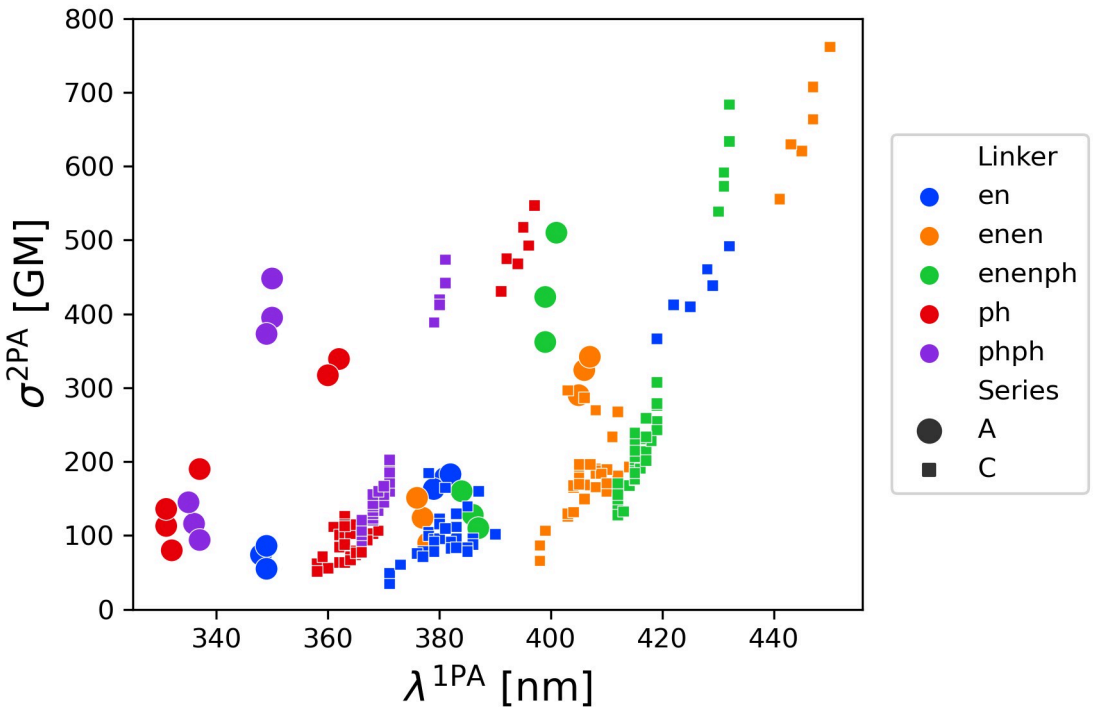

Figure 4. Correlation between λ^{1PA} and σ^{2PA} considering different linkers for series **A** and **C**. R=C_6H_4-OMe and C_6H_4-NMe_2 substituents were excluded from the **A** series for the sake of consistency with **C** derivatives.

© 2022 The Authors. ChemPhotoChem published by Wiley-VCH GmbH

23670932, 2022, 10, Downloaded from https://chemistry-europe.onlinelibrary.wiley.com/doi/10.1002/cptc.202200137 by Ifp Energies Nouvelles Compabilité Fournisseurs, Wiley Online Library on [09/11/2022]. See the Terms and Conditions (https://onlinelibrary.wiley.com/terms-and-conditions) on Wiley Online Library for rules of use; OA articles are governed by the applicable Creative Commons License

σ^{2PA} between lower and upper parts for **C** are related to the nature of the R" group (see Figure 5). Therefore, the strong donating ability of the amino group in the R" position is the key to maximize the 2PA cross-section for **C** dyes. As seen from the Figure 4, strong accepting character of the substituent R and weaker donating methoxy on the opposite branch (R′ substituent) generally secures larger σ^{2PA}. Therefore, we can conclude that for series **C** the most effective substitution aiming to increase the σ^{2PA} are the following: R being strong acceptor, R′ – weak donor and R" – strong donor.

Finally, we would wish to provide some further "chemical" discussion together with some design analyses. Given the above results and the easier synthetic access to the **A** and **B** dyes than the **C** ones, we discard the latter derivatives from our discussion below. The central acceptor core in the **A** and **B** dyes topologically correspond to the superposition of the quinoline and isoquinoline derivatives where the aromatic benzo ring is replaced by the one BF_2-carrying ring (Figure 6). The conjugation pattern in quinoline and isoquinoline differs, and the same applies to their photophysical properties, with e.g., a ϕ^{fl} of 0.94 for the OMe-quinoline[57] but 0.31 "only" for the 1-OMe-isoquinoline.[58] It is clearly hoped that the designed dyes would have large ϕ^{fl}.

Another interesting aspect is that, as can be seen in Table S1 and S2, the swap of the substituents from R = OMe, R′ = NMe_2 to R = NMe_2, R′ = OMe significantly boosts the CT properties. As shown in Figure S4 in the SI, this can be intuitively interpreted: the branch carrying R features a larger topological D–A distance than the R′ branch. We also note that the donation from NMe_2 at R towards the core is a *para*-like efficient interaction whereas its equivalent from R′ is less as it is *meta*-like.

The consideration of low- or high-response groups (*vide supra*) provided the following conclusions: a) independently of substitutions, ca. 55–65% of the dyes are classified in the second group with **enen**, **enenph**, and **phphp** linkers, while ca. 80% (50%) of the compounds having an **en** (**ph**) linker fall in the former group; b) for most **enen** and **phph** systems, the -NMe_2 group is required to obtain large cross-sections; c) all compounds bearing **enenph** or **phph** linkers and carrying at least one -NMe_2 group yield high responses. Those observations suggest that at least one amino group needs to be present in the synthetic design, though we recall that the methoxy group, while less potent, is advantageously insensitive to protonation in acidic media.

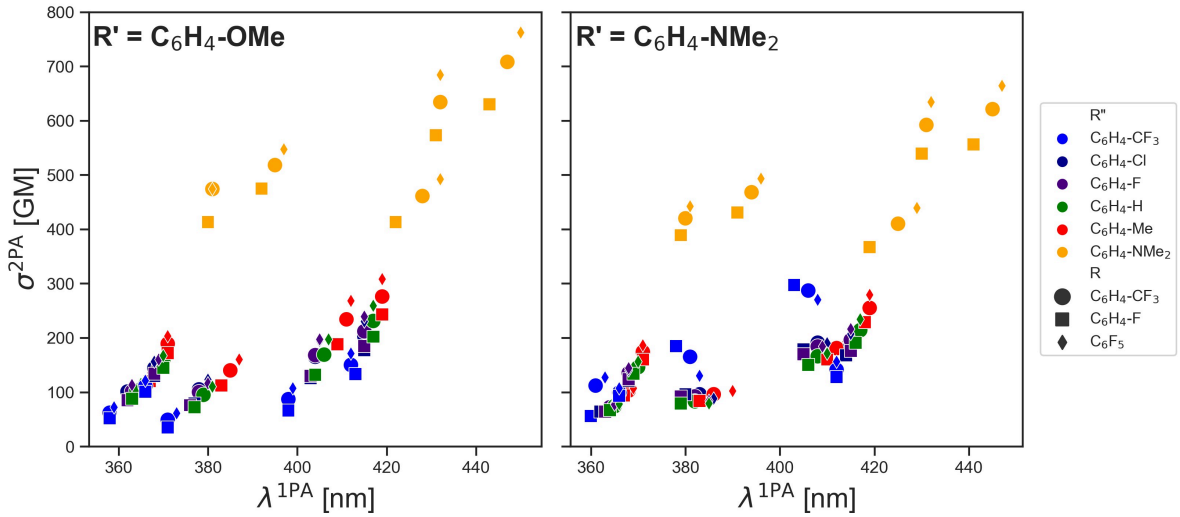

Figure 5. λ^{1PA} and σ^{2PA} decomposed by R, R′ and R" substituents for series **C**.

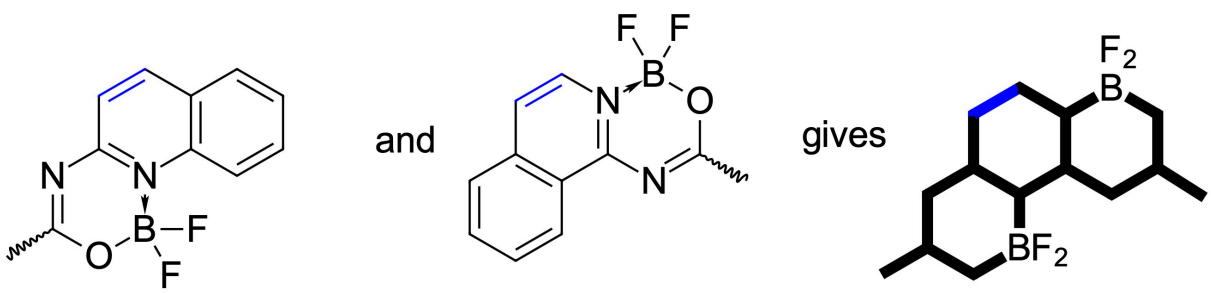

Figure 6. The superposition of topology of quinolines and 1-isoquinolines leading to the bis-BF_2 acceptor core.

© 2022 The Authors. ChemPhotoChem published by Wiley-VCH GmbH

23670932, 2022, 10, Downloaded from https://chemistry-europe.onlinelibrary.wiley.com/doi/10.1002/cptc.202200137 by Ifp Energies Nouvelles Compabilité Fournisseurs, Wiley Online Library on [09/11/2022]. See the Terms and Conditions (https://onlinelibrary.wiley.com/terms-and-conditions) on Wiley Online Library for rules of use; OA articles are governed by the applicable Creative Commons License

Conclusions

We presented a theoretical study of the 2PA properties of 280 large-sized dyes containing the difluoroborate group and split in three series (**A**, **B** and **C**). Our aim was to establish structure-properties relationships helping maximizing the 2PA cross-section in large conjugated compounds. Indeed properly functionalized BF_2-containing molecules are particularly interesting for the biomedical application, *e.g.*, as 2PA-excited fluorescent probes, due to their numerous beneficial properties, *i.e.*, solubility and stability in lipids and water combined to valuable photophysical properties in these environments, notably large emission quantum yields. We benefited from the theoretical advances in the field and performed quantum-chemical calculation of 1PA and 2PA properties using a TD-DFT approach relying on a range-separated hybrid functional.

Among the studied series, dyes of the **B** family differ by the decrease of the conjugation between the two BF_2 heterocycles while compounds of the **C** group possess an additional branch bearing various substituents as compared to **A** derivatives. We evaluated the influence of the core modifications (**A** *vs* **B**), multi-branching (**A** *vs* **C**), nature and size of π-conjugated bridges, as well as donor and acceptor strength of the peripheral substituents. Our results hint that vinylene linkers (**enen** and **enenph**) are the most effective in maximizing σ^{2PA} and redshifting λ^{1PA} irrespective of the selected core, while aromatic π-conjugated bridges (**ph** and **phph**) induce increases of σ^{2PA} for some specific derivatives of the **A** and **B** series only. More importantly, most of the compounds considered here present a λ^{1PA} larger than 350 nm which positions the 2PA peak within the first biological window (700–950 nm). Of course, we performed gas phase calculations, but it is known that most BODIPY and fluoroborate derivatives show limited solvatochromism[59,60] so one does not expect large changes of band positions in solution. Our simulation shows that a conceptually simple modification, *i.e.*, removing of a double bond in the core lead to **B** derivatives, induces noticeable increases of λ^{1PA}, σ^{2PA}, and CT parameters (D_{CT}, q_{CT} and μ_{CT}) as compared to their fully conjugated **A** counterparts. More importantly the most effective σ^{2PA} responses, considering the normalized 2PA cross-section (σ^{2PA}/N_e), are obtained for **B**-derivatives having **en** and **enen** linkers. In both **A** and **B** series we examined different variations of R and R′ substituents (see Figure 1) and concluded that large σ^{2PA} can be obtained with asymmetric substitution: strong donor and acceptor groups or strong and weak donor moieties. The addition of the new branch in series **C** results in significant bathochromic shifts of the 1PA wavelength and larger σ^{2PA} as compared to **A**-derivatives. However, the increase of σ^{2PA}/N_e for some of most molecules in series **C** in comparison with **B**-derivatives is not significant, except when **en** and **enen** linkers are used, as these deliver larger σ^{2PA} and σ^{2PA}/N_e values for **C**-dyes. In terms of substitution we observed that maximizing σ^{2PA} for series **C** requires R being strong acceptor, R′ a weak donor, and R" a strong donor. We believe that design strategies formulated herein for maximizing the 2PA cross-section using theoretical approach will be valuable for the development of the efficient 2PA absorbing dyes, as most of the dyes presented here have been conceived with an eye on synthetic accessibility.

Computational Details

All the quantum-chemical calculations are performed in gas phase, considering 280 dyes divided into three groups: **A**, **B**, and **C** as explained in the Introduction. The geometries of all compounds are optimized at the CAM–B3LYP/6-31G(d)[30,61,62] using the Gaussian 16 program.[63] We apply so-called *tight* convergence criteria for the energy gradients and select a pruned (99,590) DFT integration grid during the geometry optimization procedure. Frequency calculations, performed at the very same level of theory, confirm that all optimized structures are true minima. The calculations of the spectroscopic properties are carried out on the optimized geometries using the same CAM–B3LYP functional and the smallest Pople's basis set including both polarization and diffuse functions, namely 6–31+G(d),[64,65] using the Gamess-US program.[29] More specifically, the two-photon absorption cross-section are computed as:

$$\sigma^{2PA}(\omega) = \frac{4\pi^3 \alpha a_0^5 \omega^2}{c} g(2\omega)\delta^{2PA}, \quad (1)$$

where ω is the angular frequency of photon, so that $2\hbar\omega$ corresponds to the transition energy to the excited state (denoted hereafter as $\hbar\omega_f$); α is the fine structure constant; c is the speed of light; a_0 is the Bohr radius; and δ^{2PA} is the orientationally-averaged two-photon transition strength.[66] In this study, reporting gas-phase 2PA properties, we apply a Lorentzian profile to represent broadening function of two-photon absorption band:

$$g(2\omega) = \frac{1}{\pi} \frac{\frac{1}{2}\Gamma_f}{(\omega_f - 2\omega)^2 + (\frac{1}{2}\Gamma_f)^2}. \quad (2)$$

Note that Γ_f in the above equation corresponds to full width at half maximum. For $\omega_f = 2\omega$ one obtains:

$$\sigma^{2PA}(\omega = \frac{1}{2}\omega_f) = \frac{8\pi^2 \alpha a_0^5 \omega^2}{c\Gamma_f}\delta^{2PA}. \quad (3)$$

All values of σ^{2PA} reported in this study are obtained with Γ_f= 0.1 eV, which is a standard value in the field. We also determine the charge-transfer (CT) parameters using Le Bahers metric,[67,68] namely the CT distance (D_{CT}), that allows to define the spatial separation between the electron and the hole associated to a given transition, the amount of transferred charge from the ground to the excited states (q_{CT}), and the variation of dipole moment between the ground and the excited states (μ_{CT}). The Gaussian program is used for computing these topological signatures.

Supporting Information

Additional correlation graphs between the two-photon absorption cross-section, the oscillator strength, the CT parameters; normalized two-photon absorption cross-section for all series; density difference plots and graphical representation of charge transfer in selected molecules (pdf). Raw data (xls). Link to Cartesian coordinates.

© 2022 The Authors. ChemPhotoChem published by Wiley-VCH GmbH

23670932, 2022, 10, Downloaded from https://chemistry-europe.onlinelibrary.wiley.com/doi/10.1002/cptc.202200137 by Ifp Energies Nouvelles Compabilité Fournisseurs, Wiley Online Library on [09/11/2022]. See the Terms and Conditions (https://onlinelibrary.wiley.com/terms-and-conditions) on Wiley Online Library for rules of use; OA articles are governed by the applicable Creative Commons License

Acknowledgements

We cordially thank Miss E. F. Petrusevich for preparing the graphical abstract. The Wroclaw and Nantes teams are indebted to the CNRS for supporting their collaboration in the framework of the ABSOLUTA-IEA grant. I.K and D.J. acknowledge financial support from the French National Research Agency (BSE-Forces, ANR-20-CE29-0005). R.Z. and B.O. gratefully acknowledges the support from the National Science Centre, Poland (Grant No. 2017/26/M/ST5/00327). Authors used computational resources generously provided by the Wroclaw Center for Networking and Supercomputing as well as the CCIPL computational center installed in Nantes.

Conflict of Interest

The authors declare no conflict of interest.

Data Availability Statement

The data that support the findings of this study are available in the supplementary material of this article.

Keywords: ab initio calculations · density functional calculations · dyes/pigments · electronic spectroscopy · two-photon absorption

[1] M. Göppert-Mayer, *Ann. Phys.* **1931**, *401*, 273–294.
[2] W. Kaiser, C. G. B. Garrett, *Phys. Rev. Lett.* **1961**, *7*, 229–231.
[3] S. Maruo, O. Nakamura, S. Kawata, *Opt. Lett.* **1997**, *22*, 132–134.
[4] K. sup Lee, R. H. Kim, D.-Y. Yang, S. hu Park, *Prog. Polym. Sci.* **2008**, *33*, 631–681.
[5] J. H. Strickler, W. W. Webb, *Opt. Lett.* **1991**, *16*, 1780–1782.
[6] S. Pascal, S. David, C. Andraud, O. Maury, *Chem. Soc. Rev.* **2021**, *50*, 6613–6658.
[7] H. M. Kim, B. R. Cho, *Chem. Rev.* **2015**, *115*, 5014–5055.
[8] S. Yao, K. D. Belfield, *Eur. J. Org. Chem.* **2012**, *2012*, 3199–3217.
[9] Y. Shen, A. J. Shuhendler, D. Ye, J.-J. Xu, H.-Y. Chen, *Chem. Soc. Rev.* **2016**, *45*, 6725–6741.
[10] J. Olsen, P. Jørgensen, *J. Chem. Phys.* **1985**, *82*, 3235–3264.
[11] H. Hettema, H. J. A. Jensen, P. Jørgensen, J. Olsen, *J. Chem. Phys.* **1992**, *97*, 1174–1190.
[12] C. Hättig, O. Christiansen, P. Jørgensen, *J. Chem. Phys.* **1998**, *108*, 8331–8354.
[13] C. Hättig, P. Jørgensen, *J. Chem. Phys.* **1998**, *109*, 9219–9236.
[14] P. Sałek, O. Vahtras, J. Guo, Y. Luo, T. Helgaker, H. Ågren, *Chem. Phys. Lett.* **2003**, *374*, 446–452.
[15] M. J. Paterson, O. Christiansen, F. Pawłowski, P. Jørgensen, C. Hättig, T. Helgaker, P. Sałek, *J. Chem. Phys.* **2006**, *124*, 054322.
[16] D. H. Friese, C. Hättig, K. Ruud, *Phys. Chem. Chem. Phys.* **2012**, *14*, 1175–1184.
[17] F. Zahariev, M. S. Gordon, *J. Chem. Phys.* **2014**, *140*, 18A523.
[18] K. D. Nanda, A. I. Krylov, *J. Chem. Phys.* **2015**, *142*, 064118.
[19] M. T. P. Beerepoot, D. H. Friese, N. H. List, J. Kongsted, K. Ruud, *Phys. Chem. Chem. Phys.* **2015**, *17*, 19306–19314.
[20] S. M. Parker, D. Rappoport, F. Furche, *J. Chem. Theory Comput.* **2018**, *14*, 807–819.
[21] M. T. P. Beerepoot, M. M. Alam, J. Bednarska, W. Bartkowiak, K. Ruud, R. Zaleśny, *J. Chem. Theory Comput.* **2018**, *14*, 3677–3685.
[22] D. Grabarek, T. Andruniów, *J. Chem. Theory Comput.* **2019**, *15*, 490–508.
[23] M. Chołuj, M. M. Alam, M. T. P. Beerepoot, S. P. Sitkiewicz, E. Matito, K. Ruud, R. Zaleśny, *J. Chem. Theory Comput.* **2022**, *18*, 1046–1060.
[24] DALTON, a molecular electronic structure program, Release 2014.0 (2015), see http://daltonprogram.org.
[25] K. Aidas, C. Angeli, K. L. Bak, V. Bakken, R. Bast, L. Boman, O. Christiansen, R. Cimiraglia, S. Coriani, P. Dahle, E. K. Dalskov, U. Ekström, T. Enevoldsen, J. J. Eriksen, P. Ettenhuber, B. Fernández, L. Ferrighi, H. Fliegl, L. Frediani, K. Hald, A. Halkier, C. Hättig, H. Heiberg, T. Helgaker, A. C. Hennum, H. Hettema, E. Hjertenæs, S. Høst, I.-M. Høyvik, M. F. Iozzi, B. Jansík, H. J. A. Jensen, D. Jonsson, P. Jørgensen, J. Kauczor, S. Kirpekar, T. Kjærgaard, W. Klopper, S. Knecht, R. Kobayashi, H. Koch, J. Kongsted, A. Krapp, K. Kristensen, A. Ligabue, O. B. Lutnæs, J. I. Melo, K. V. Mikkelsen, R. H. Myhre, C. Neiss, C. B. Nielsen, P. Norman, J. Olsen, J. M. H. Olsen, A. Osted, M. J. Packer, F. Pawlowski, T. B. Pedersen, P. F. Provasi, S. Reine, Z. Rinkevicius, T. A. Ruden, K. Ruud, V. V. Rybkin, P. Sałek, C. C. M. Samson, A. S. de Merás, T. Saue, S. P. A. Sauer, B. Schimmelpfennig, K. Sneskov, A. H. Steindal, K. O. Sylvester-Hvid, P. R. Taylor, A. M. Teale, E. I. Tellgren, D. P. Tew, A. J. Thorvaldsen, L. Thøgersen, O. Vahtras, M. A. Watson, D. J. D. Wilson, M. Ziolkowski, H. Ågren, *WIREs Comput. Mol. Sci.* **2014**, *4*, 269–284.
[26] Y. Shao, Z. Gan, E. Epifanovsky, A. T. Gilbert, M. Wormit, J. Kussmann, A. W. Lange, A. Behn, J. Deng, X. Feng, D. Ghosh, M. Goldey, P. R. Horn, L. D. Jacobson, I. Kaliman, R. Z. Khaliullin, T. Kuś, A. Landau, J. Liu, E. I. Proynov, Y. M. Rhee, R. M. Richard, M. A. Rohrdanz, R. P. Steele, E. J. Sundstrom, H. L. Woodwork III, P. M. Zimmerman, D. Zuev, B. Albrecht, E. Alguire, B. Austin, G. J. O. Beran, Y. A. Bernard, E. Berquist, K. Brandhorst, K. B. Bravaya, S. T. Brown, D. Casanova, C.-M. Chang, Y. Chen, S. H. Chien, K. D. Closser, D. L. Crittenden, M. Diedenhofen, R. A. D. Jr., H. Do, A. D. Dutoi, R. G. Edgar, S. Fatehi, L. Fusti-Molnar, A. Ghysels, A. Golubeva-Zadorozhnaya, J. Gomes, M. W. Hanson-Heine, P. H. Harbach, A. W. Hauser, E. G. Hohenstein, Z. C. Holden, T.-C. Jagau, H. Ji, B. Kaduk, K. Khistyaev, J. Kim, J. Kim, R. A. King, P. Klunzinger, D. Kosenkov, T. Kowalczyk, C. M. Krauter, K. U. Lao, A. D. Laurent, K. V. Lawler, S. V. Levchenko, C. Y. Lin, F. Liu, E. Livshits, R. C. Lochan, A. Luenser, P. Manohar, S. F. Manzer, S.-P. Mao, N. Mardirossian, A. V. Marenich, S. A. Maurer, N. J. Mayhall, E. Neuscamman, C. M. Oana, R. Olivares-Amaya, D. P. O'Neill, J. A. Parkhill, T. M. Perrine, R. Peverati, A. Prociuk, D. R. Rehn, E. Rosta, N. J. Russ, S. M. Sharada, S. Sharma, D. W. Small, A. Sodt, T. Stein, D. Stück, Y.-C. Su, A. J. Thom, T. Tsuchimochi, V. Vanovschi, L. Vogt, O. Vydrov, T. Wang, M. A. Watson, J. Wenzel, A. White, C. F. Williams, J. Yang, S. Yeganeh, S. R. Yost, Z.-Q. You, I. Y. Zhang, X. Zhang, Y. Zhao, B. R. Brooks, G. K. Chan, D. M. Chipman, C. J. Cramer, W. A. Goddard III, M. S. Gordon, W. J. Hehre, A. Klamt, H. F. Schaefer III, M. W. Schmidt, C. D. Sherrill, D. G. Truhlar, A. Warshel, X. Xu, A. Aspuru-Guzik, R. Baer, A. T. Bell, N. A. Besley, J.-D. Chai, A. Dreuw, B. D. Dunietz, T. R. Furlani, S. R. Gwaltney, C.-P. Hsu, Y. Jung, J. Kong, D. S. Lambrecht, W. Liang, C. Ochsenfeld, V. A. Rassolov, L. V. Slipchenko, J. E. Subotnik, T. V. Voorhis, J. M. Herbert, A. I. Krylov, P. M. Gill, M. Head-Gordon, *Mol. Phys.* **2015**, *113*, 184–215.
[27] M. de Wergifosse, C. G. Elles, A. I. Krylov, *J. Chem. Phys.* **2017**, *146*, 174102.
[28] TURBOMOLE V7.0 2015, a development of University of Karlsruhe and Forschungszentrum Karlsruhe GmbH, 1989–2007, TURBOMOLE GmbH, since 2007; available from http://www.turbomole.com (Last accessed 01 Apr. 17).
[29] M. W. Schmidt, K. K. Baldridge, J. A. Boatz, S. T. Elbert, M. S. Gordon, J. H. Jensen, S. Koseki, N. Matsunaga, K. A. Nguyen, S. Su, T. L. Windus, M. Dupuis, J. A. Montgomery, *J. Comput. Chem.* **1993**, *14*, 1347–1363.
[30] T. Yanai, D. P. Tew, N. C. Handy, *Chem. Phys. Lett.* **2004**, *393*, 51–57.
[31] B. Le Guennic, D. Jacquemin, *Acc. Chem. Res.* **2015**, *48*, 530–537.
[32] M. R. Momeni, A. Brown, *J. Chem. Theory Comput.* **2015**, *11*, 2619–2632.
[33] R. Berraud-Pache, F. Neese, G. Bistoni, R. Izsák, *J. Phys. Chem. Lett.* **2019**, *10*, 4822–4828.
[34] S. David, H.-J. Chang, C. Lopes, C. Brännlund, B. Le Guennic, G. Berginc, E. Van Stryland, M. V. Bondar, D. Hagan, D. Jacquemin, C. Andraud, O. Maury, *Chem. Eur. J.* **2021**, *27*, 3517–3525.
[35] M. M. Alam, M. Chattopadhyaya, S. Chakrabarti, *Phys. Chem. Chem. Phys.* **2012**, *14*, 1156–1165.
[36] M. T. P. Beerepoot, M. M. Alam, J. Bednarska, W. Bartkowiak, K. Ruud, R. Zaleśny, *J. Chem. Theory Comput.* **2018**, *14*, 3677–3685.
[37] L.-C. Cheng, N. G. Horton, K. Wang, S.-J. Chen, C. Xu, *Biomed. Express* **2014**, *5*, 3427–3433.
[38] M. Pawlicki, H. Collins, R. Denning, H. Anderson, *Angew. Chem. Int. Ed.* **2009**, *48*, 3244–3266; *Angew. Chem.* **2009**, *121*, 3292–3316.
[39] L. Xu, J. Zhang, L. Yin, X. Long, W. Zhang, Q. Zhang, *J. Mater. Chem. C* **2020**, *8*, 6342–6349.

© 2022 The Authors. ChemPhotoChem published by Wiley-VCH GmbH

23670932, 2022, 10, Downloaded from https://chemistry-europe.onlinelibrary.wiley.com/doi/10.1002/cptc.202200137 by Ifp Energies Nouvelles Compabilité Fournisseurs, Wiley Online Library on [09/11/2022]. See the Terms and Conditions (https://onlinelibrary.wiley.com/terms-and-conditions) on Wiley Online Library for rules of use; OA articles are governed by the applicable Creative Commons License

[40] L. Xu, W. Lin, B. Huang, J. Zhang, X. Long, W. Zhang, Q. Zhang, *J. Mater. Chem. C* **2021**, *9*, 1520–1536.
[41] M. Albota, D. Beljonne, J.-L. Brédas, J. E. Ehrlich, J.-Y. Fu, A. A. Heikal, S. E. Hess, T. Kogej, M. D. Levin, S. R. Marder, D. McCord-Maughon, J. W. Perry, H. Röckel, M. Rumi, G. Subramaniam, W. W. Webb, X.-L. Wu, C. Xu, *Science* **1998**, *281*, 1653–1656.
[42] C. Katan, F. Terenziani, O. Mongin, M. H. V. Werts, L. Porrès, T. Pons, J. Mertz, S. Tretiak, M. Blanchard-Desce, *J. Phys. Chem. A* **2005**, *109*, 3024–3037.
[43] Z. Shi, X. Han, W. Hu, H. Bai, B. Peng, L. Ji, Q. Fan, L. Li, W. Huang, *Chem. Soc. Rev.* **2020**, *49*, 7533–7567.
[44] T. Govender, L. Ramanna, I. Rawat, F. Bux, *Bioresour. Technol.* **2012**, *114*, 507–511.
[45] D. Kand, P. Liu, M. X. Navarro, L. J. Fischer, L. Rousso-Noori, D. Friedmann-Morvinski, A. H. Winter, E. W. Miller, R. Weinstain, *J. Am. Chem. Soc.* **2020**, *142*, 4970–4974.
[46] J. Pliquett, A. Dubois, C. Racoeur, N. Mabrouk, S. Amor, R. Lescure, A. Bettaïeb, B. Collin, C. Bernhard, F. Denat, P. S. Bellaye, C. Paul, E. Bodio, C. Goze, *Bioconjugate Chem.* **2019**, *30*, 1061–1066.
[47] O. Coban, M. Burger, M. Laliberte, A. Ianoul, L. J. Johnston, *Langmuir* **2007**, *23*, 6704–6711.
[48] A. D'Aléo, D. Gachet, V. Heresanu, M. Giorgi, F. Fages, *Chem. Eur. J.* **2012**, *18*, 12764–12772.
[49] Y. Kubota, K. Kasatani, H. Takai, K. Funabiki, M. Matsui, *Dalton Trans.* **2015**, *44*, 3326–3341.
[50] L. Kong, Z. Huang, S.-S. Zhang, J. Song, Y.-Y. Zhang, X.-Y. Bai, J.-X. Yang, L. Li, *Chem. Commun.* **2020**, *56*, 571–574.
[51] J. Bednarska, R. Zaleśny, M. Wielgus, B. Jędrzejewska, R. Puttreddy, K. Rissanen, W. Bartkowiak, H. Ågren, B. Ośmiałowski *Phys. Chem. Chem. Phys.* **2017**, *19*, 5705–5708.
[52] B. Ośmiałowski, E. F. Petrusevich, M. A. Antoniak, I. Grela, M. A. Bin Jassar, M. Nyk, J. M. Luis, B. Jędrzejewska, R. Zaleśny, D. Jacquemin, *J. Phys. Chem. Lett.* **2020**, *11*, 5920–5925.
[53] B. Ośmiałowski, E. F. Petrusevich, K. C. Nawrot, B. K. Paszkiewicz, M. Nyk, J. Zielak, B. Jędrzejewska, J. M. Luis, D. Jacquemin, R. Zaleśny, *J. Mater. Chem. C* **2021**, *9*, 6225–6233.
[54] R. Zaleśny, N. Szczotka, A. Grabarz, B. Ośmiałowski, D. Jacquemin, *ChemPhotoChem* **2019**, *3*, 719–726.
[55] A. M. Grabarz, A. D. Laurent, B. Jędrzejewska, A. Zakrzewska, D. Jacquemin, B. Ośmiałowski, *J. Org. Chem.* **2016**, *81*, 2280–2292.
[56] B. Jędrzejewska, A. Zakrzewska, G. Mlostoń, S. Budzák, K. Mroczynska, A. M. Grabarz, M. A. Kaczorowska, D. Jacquemin, B. Ośmiałowski, *J. Phys. Chem. A* **2016**, *120*, 4116–4123.
[57] A. Zakrzewska, R. Zaleśny, E. Kolehmainen, B. Ośmiałowski, B. Jędrzejewska, H. Ågren, M. Pietrzak, *Dyes Pigm.* **2013**, *99*, 957–965.
[58] B. Ośmiałowski, A. Zakrzewska, B. Jędrzejewska, A. Grabarz, R. Zaleśny, W. Bartkowiak, E. Kolehmainen, *J. Org. Chem.* **2015**, *80*, 2072–2080.
[59] B. Jędrzejewska, A. Grabarz, W. Bartkowiak, B. Ośmiałowski, *Spectrochim. Acta Part A* **2018**, *199*, 86–95.
[60] J. A. González-Vera, F. Lv, D. Escudero, A. Orte, X. Guo, E. Hao, E. M. Talavera-Rodriguez, L. Jiao, N. Boens, M. J. Ruedas-Rama, *Dyes Pigm.* **2020**, *182*, 108510.
[61] P. C. Hariharan, J. A. Pople, *Theor. Chim. Acta* **1973**, *28*, 213–222.
[62] M. M. Francl, W. J. Pietro, W. J. Hehre, J. S. Binkley, M. S. Gordon, D. J. DeFrees, J. A. Pople, *J. Chem. Phys.* **1982**, *77*, 3654–3665.
[63] M. J. Frisch, G. W. Trucks, H. B. Schlegel, G. E. Scuseria, M. A. Robb, J. R. Cheeseman, G. Scalmani, V. Barone, G. A. Petersson, H. Nakatsuji, X. Li, M. Caricato, A. V. Marenich, J. Bloino, B. G. Janesko, R. Gomperts, B. Mennucci, H. P. Hratchian, J. V. Ortiz, A. F. Izmaylov, J. L. Sonnenberg, D. Williams-Young, F. Ding, F. Lipparini, F. Egidi, J. Goings, B. Peng, A. Petrone, T. Henderson, D. Ranasinghe, V. G. Zakrzewski, J. Gao, N. Rega, G. Zheng, W. Liang, M. Hada, M. Ehara, K. Toyota, R. Fukuda, J. Hasegawa, M. Ishida, T. Nakajima, Y. Honda, O. Kitao, H. Nakai, T. Vreven, K. Throssell, J. A. Montgomery, Jr., J. E. Peralta, F. Ogliaro, M. J. Bearpark, J. J. Heyd, E. N. Brothers, K. N. Kudin, V. N. Staroverov, T. A. Keith, R. Kobayashi, J. Normand, K. Raghavachari, A. P. Rendell, J. C. Burant, S. S. Iyengar, J. Tomasi, M. Cossi, J. M. Millam, M. Klene, C. Adamo, R. Cammi, J. W. Ochterski, R. L. Martin, K. Morokuma, O. Farkas, J. B. Foresman, D. J. Fox, Gaussian 2016, gaussian Inc. Wallingford CT 2016.
[64] W. J. Hehre, R. Ditchfield, J. A. Pople, *J. Chem. Phys.* **1972**, *56*, 2257–2261.
[65] T. Clark, J. Chandrasekhar, G. W. Spitznagel, P. V. R. Schleyer, *J. Comput. Chem.* **1983**, *4*, 294–301.
[66] P. Monson, W. McClain, *J. Chem. Phys.* **1970**, *53*, 29–37.
[67] T. Le Bahers, C. Adamo, I. Ciofini, *J. Chem. Theory Comput.* **2011**, *7*, 2498–2506.
[68] D. Jacquemin, T. L. Bahers, C. Adamo, I. Ciofini, *Phys. Chem. Chem. Phys.* **2012**, *14*, 5383–5388.

Manuscript received: May 18, 2022
Revised manuscript received: June 22, 2022
Accepted manuscript online: June 23, 2022
Version of record online: August 5, 2022

© 2022 The Authors. ChemPhotoChem published by Wiley-VCH GmbH

23670932, 2022, 10, Downloaded from https://chemistry-europe.onlinelibrary.wiley.com/doi/10.1002/cptc.202200137 by Ifp Energies Nouvelles Compabilité Fournisseurs, Wiley Online Library on [09/11/2022]. See the Terms and Conditions (https://onlinelibrary.wiley.com/terms-and-conditions) on Wiley Online Library for rules of use; OA articles are governed by the applicable Creative Commons License